

Chapter 9

Solid Solution $Hg_{1-x}Mn_xTe$ – Based Mid Infrared Schottky Diodes

I. V. Ivanchenko, V. M. Godovanyuk, M. L. Kovalchuk, S. E. Ostapov, S. Yu. Paranchich, N. A. Popenko, I. M. Rarenko

Abstract The investigations of electric and photoelectric parameters of the semiconductor solid solutions $Hg_{1-x}Mn_xTe$ -based Schottky photodiodes being applicable for $\lambda = 3 \div 5 \mu\text{m}$ and $\lambda = 8 \div 14 \mu\text{m}$ regions are presented in this paper. These diodes overlap the spectral range which is wider than that of $InSb$ -based photodiodes and demonstrate the better perfection of the crystal structure in comparison with the $HgCdTe$ -based photodiodes.

9.1 Introduction

Nowadays, there has been a significant progress in THz generation and detection due to achievements in the nanotechnology and small-scale semiconductor industry [1, 2]. As regards the detection problems, the research-and-development activities of numerous research teams were focused during the last two decades on the search for alternative materials to the well-known $HgCdTe$ - and $InSb$ -based photodiodes for detecting IR radiation in the spectral ranges $\lambda = 3 \div 5 \mu\text{m}$ and $\lambda = 8 \div 14 \mu\text{m}$. But the main drawback of $HgCdTe$ compounds is a weakness of the crystal $Hg - Te$ bond, which leads to the intrinsic point defects formation especially under mechanical treatment and thermal shock conditions. The substitution of Cd -atoms with Mn or Zn ones gives rise to the significant improvement of the crystal perfection as well as to the surface and interfaces quality.

I. V. Ivanchenko, N. A. Popenko
Usikov Institute for Radiophysics and Electronics of NASU, 12 Ak. Proskya st., Kharkov, Ukraine, e-mail: ireburan@yahoo.com

V. M. Godovanyuk, M. L. Kovalchuk, S. E. Ostapov, S. Yu. Paranchich, I. M. Rarenko
Chernivtsi National University, Chernivtsi, Ukraine, e-mail: sergey.ostapov@gmail.com

9.2 Crystal Growth

The $Hg_{1-x}Mn_xTe$ crystals ($0.1 \leq x \leq 0.125$) as a substrate of photodiodes were grown by the modified zone-melting method after alloying suitable components with a high purity. The substrates were cut out from these crystals and annealed in the mercury vapors at temperatures $180^\circ\text{C} \div 240^\circ\text{C}$ for providing n - or p -type of conductivity and the suitable concentration of equilibrium electrons or holes, respectively. After chemical-mechanical treatment and consequent purification by the argon atoms bombardment, the aluminum film with the thickness of 20 nm was deposited for Schottky diodes preparation.

9.3 Differences and Advantages

The main drawback of $HgCdTe$ -based photodiodes is that, the carrier's mobility in the near-surface region decreases essentially after mechanical treatment of the crystals due to the plastic deformation this area with the simultaneous formation of the intrinsic electroactive point defects. There is the same effect after multiple thermo shock cycles of these crystals ($+60^\circ\text{C} \div -190^\circ\text{C}$ in 3–5 s for each cycle). The substitution of the Cd atoms with the Mn ones in the solid solution $HgCdTe$ gives rise not only to the significant improvement of the crystal structure (in this case the block size increases while the disordered orientation of those and the dislocation density decreases) but to the improvement of both the surface conductivity and the interface quality. In this respect, the diluted magnetic semiconductors $HgMnTe$ seem to be very attractive ones for this purpose from their practical application point of view.

The advantages of $HgMnTe$ compound let us to produce the high quality Schottky barrier by coating the thin semitransparent metallic layer (200–300) Å on the semiconductor substrate with the further usual photolithographic process. As the result, we obtain the required illuminated surfaces.

9.4 Calculations

By using Runge–Kutta method and solving appropriate Poisson equations we have numerically got a charge density distribution in the given structure, as well as a behavior of the electric field strength and potential in the contact area of the semiconductor with the metal. From the calculations it has been shown that in narrow-gap $Hg_{1-x}Mn_xTe$ semiconductors, having the band-gap energy suitable for employing those as the photodetector substrates, the charge is not to be constant in the middle of the depletion zone due to the influence of free carriers. It gives rise to the deflection in the coordinate distribution of the electric field strength from the linear dependence and the potential from the quadratic one that does not allow for employing well-known formulas which do not take into account the influence of free

carriers. At the same time, by using the joint diffusion-diode theory we are able to calculate the currents flowing in the Schottky photodiode. The comparison of the generation-recombination current being calculated according to the well-known formula

$$J_{gr} = e \int U(x, V) dx, \quad (9.1)$$

with the tunnel current I

$$I = I_0 \times \int_0^{\varphi_0 - eV - E_g} \{f_p(E) - f_n(E)\} D(E) dE, \quad (9.2)$$

and with the diffusion current j , which is given by the stated below formula according to the joint diffusion-diode theorem by Crowell and Sze [3]

$$j = j_S \left(\exp\left(\frac{eV}{kT}\right) - 1 \right), \quad j_S = A^* \cdot T^2 e^{-\frac{e\varphi_0}{kT}}, \quad (9.3)$$

where A^* is the Richardson constant, shows that both the generation and recombination can not substantially effect on the current, i.e., the volt-ampere characteristic of Schottky photodiode should be described by the sum of diffusion and tunnel currents.

By taking into account the last statement, the calculated currents for the high direct biases V are strongly overestimated as compared with the measured ones more than three times. In this case we have to allow that a high band curvature gives rise to the substantial electron diffusion current. Since the hole diffusion current is proportional to the $m_h \exp[-(\varphi_0 + \Delta\mu)/kT]$, and the electron diffusion current is proportional to the $-m_e \exp[-(E_g - \Delta\mu)/kT]$, one can conclude that for the $\varphi_0 > E_g - 2\Delta\mu - kT \ln(m_e/m_h)$ the electron diffusion current exceeds the hole diffusion current. Generally, we are obliged to consider both the electron diffusion current and the hole diffusion current. As a result of everything noted above the calculated results for the tunnel and diffusion currents are shown in Fig. 9.1(a). This figure illustrates the ratio of tunnel and diffusion current components. In the cases of reverse bias and small direct bias the diffusion current is lower substantially as compared with the tunnel current.

However, with the direct bias increase the increase of tunnel current becomes slower and when V tends to the value φ_0/e , the tunnel current starts decreases that can be explained by shifting the most effective tunneling region towards the higher energies. At the same time a contribution of the diffusion current increases so that for the direct bias about 0.2–0.3 V these components become the same while for the higher direct biases the diffusion current dominates. The latest case makes possible to determine quite accurately the barrier height φ_0 for which the calculated current coincides well with the measured one in the region of high direct biases. Just as it has expected, the band curvature near the semiconductor surface becomes so high that the diffusion electron current exceeds the diffusion hole current.

So, as it follows from the calculations we can conclude that: (i) $j \ll I$ for the reverse bias and the small direct bias; (ii) when the bias increases, the increment of

the value of a quantity I becomes slower and when V reaches the φ_0/e value, I tends to the decrease; (iii) $j = I$ for $V = 0.02 - 0.03$ V, and j dominates for $V > 0.03$ V. When all the suitable parameters are known, we can calculate the volt-ampere characteristics of the $Al - Hg_{1-x}Mn_xTe$ diodes by taking into account the sum of tunnel and diffusion currents as well as by varying the manganese composition (x) and acceptor's concentration (N_a).

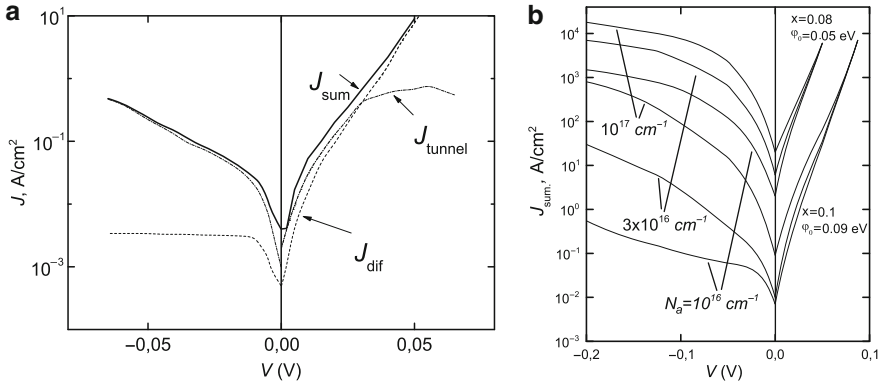


Fig. 9.1 Calculated tunnel and diffusion currents in the $Al - Hg_{1-x}Mn_xTe$ diode for $x = 0.09$, $\varphi_0 = 0.07$ eV, $N_a = 3 \cdot 10^{16} \text{ cm}^{-3}$, $T = 300$ K (a). Total currents calculated for the aforementioned parameters (b)

The results presented in Fig. 9.1(b) explain the features of the experimental characteristics of diodes. One can see that the volt-ampere characteristic undergo qualitative changes by varying the values x , φ_0 and N_a . For $x = 0.1$, $\varphi_0 = 0.09$ eV, and $N_a = 10^{16} \text{ cm}^{-3}$ the diode demonstrates good characteristics (direct current exceeds the reverse current by the several times). At the same time, for $x = 0.08$, $\varphi_0 = 0.05$ eV, and $N_a = 10^{17} \text{ cm}^{-3}$ the reverse current exceeds the direct one. The main reason of such evolution of the volt-ampere characteristic is an increase of the tunnel current as compared with the diffusion current (exceeding the reverse current over the direct one in so-called “backward diodes”, for example, in the Ge -junction [3]). As one sees from the Fig. 9.1(a), for $x = 0.09 \div 0.1$, $\varphi_0 \approx 0.07$ eV, and $N_a = (3 \div 10) \cdot 10^{16} \text{ cm}^{-3}$ the direct currents and reverse currents are the same virtually. The proposed model explain also the temperature changes of the volt-ampere characteristic of $Al - Hg_{1-x}Mn_xTe$ diodes. The calculated volt-ampere characteristic of such a diode at 77 and 300 K for $x = 0.1$, $\varphi_0 = 0.1$ eV, and $N_a = 10^{16} \text{ cm}^{-3}$ are shown in Fig. 9.2.

It can be seen that at the liquid nitrogen temperature the diode straightening is absent while at the room temperature the direct current exceeds the reverse one in the several times that is observed in the experiments. It is quite clear that by varying the diode parameters one can reach virtually a full coincidence of the calculated and experimental results.

9.5 Measurements and Discussions

The results of such calculations explain the volt-ampere characteristic features of the diodes which occur in the experiments (see Fig. 9.3).

The main detector parameter is the detectivity D^* , which is determined by the diode structure conductivity and the background radiation

$$D^* = \frac{e\eta\lambda_c}{hc} \left[\frac{4kT}{R_0A} + 2e^2\eta\Phi_B \right]^{-1/2}, \tag{9.4}$$

where η is the quantum efficiency, Φ_B is the background irradiation flow density. The parameter η is equal 0.5–0.7 and Φ_B is $5 \cdot 10^7 \text{ cm}^{-2}\text{s}^{-1}$ for $\lambda_c = 9 - 10\mu\text{m}$ at 300 K and 180° irradiation angle. The detector conductivity is expressed as a product of its differential resistance at zero displacement on the active area (so-called R_0A product).

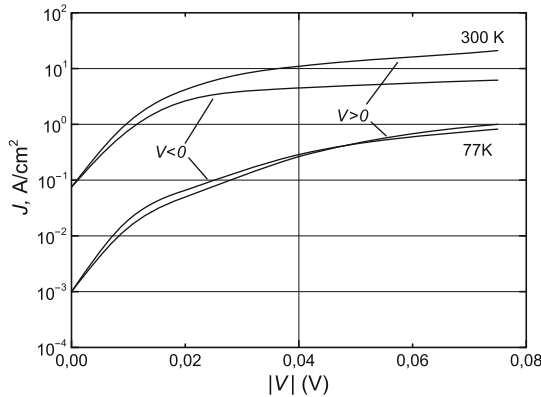


Fig. 9.2 The calculated direct and reverse currents in the $Al - Hg_{1-x}Mn_xTe$ diode for $x = 0.1$, $\varphi_0 = 0.07 \text{ eV}$, and $N_a = 10^{16} \text{ cm}^{-3}$ at 77 and 300 K

The measurement results of the differential resistance of the $Al - Hg_{1-x}Mn_xTe$ diode at two temperatures are shown in Fig. 9.4(a).

At the temperature $T = 77 \text{ K}$ and zero bias (the working conditions of such detectors) we have obtained the product value $R_0A \approx 2 \Omega \cdot \text{cm}^2$. For such R_0A value the first term in the squared bracket is approximately eight times as less than the second term. It means that the detector’s detectivity is determined by the background radiation at 77 K and 180° irradiation angle, i.e., it is close to the boundary-possible value of $D^* \approx 3.6 \cdot 10^{10} \text{ cm} \cdot \text{Hz}^{1/2} \cdot \text{W}^{-1}$ (so-called “Background-limited Infrared Photodetector”). The results of calculations point also out the enough high quality of the $Al - Hg_{1-x}Mn_xTe$ diodes as the detectors for infrared radiation. Figure 9.4(b) shows the R_0A dependence on the N_a acceptor concentration for three values: $x = 0.095$, 0.01, and 0.0105 at 77 K that corresponds to the practically important interval of the

boundary wavelengths $\lambda_c = 13, 11, \text{ and } 10 \mu\text{m}$, respectively. As can be seen from this Figure the calculated R_0A value exceeds $10 \text{ Ohm}\cdot\text{cm}^2$ for $N_a = 3 \cdot 10^{16} \text{ cm}^{-3}$ and it is larger than $2 \div 3 \Omega \cdot \text{cm}^2$ even for $N_a = (5 \div 10) \cdot 10^{16} \text{ cm}^{-3}$.

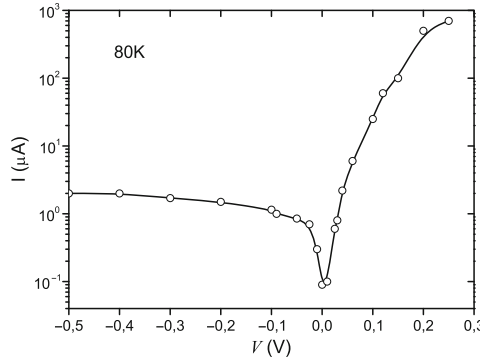


Fig. 9.3 Volt-ampere characteristic of the $Al - Hg_{1-x}Mn_xTe$ diode: measured (circles) and calculated according to the generation-recombination theory (solid line)

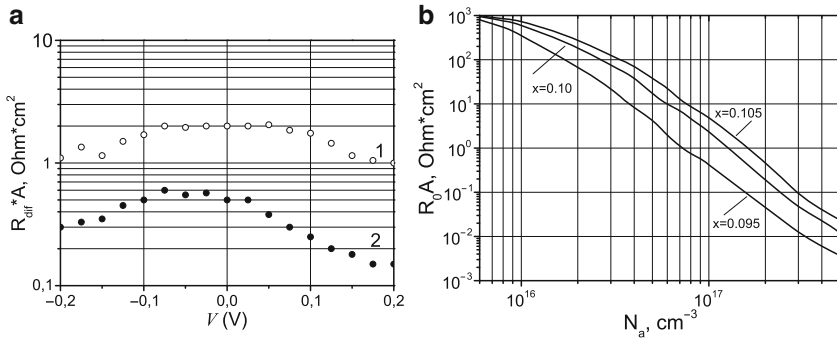


Fig. 9.4 (a) Measured R_0A product of the $Al - Hg_{0.9}Mn_{0.1}Te$ Schottky diode versus the bias voltage: 1–77 K; 2–300K; (b) Calculated R_0A product of the $Al - Hg_{1-x}Mn_xTe$ Schottky diode versus the acceptor concentration for different wavelengths at 77 K

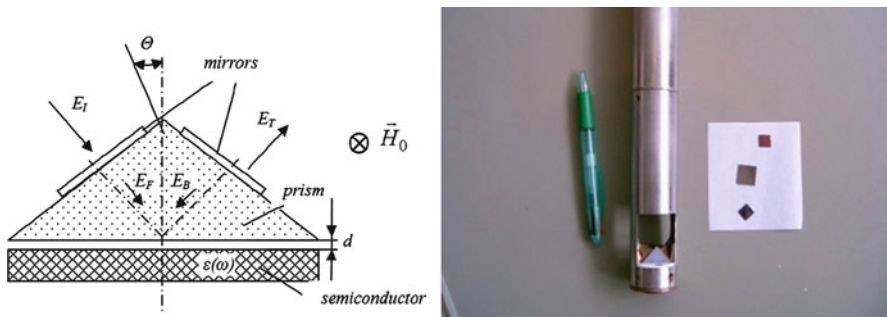


Fig. 9.5 Prism transformer of the surface EM waves (left). Measuring module (right)

As it was noted above, in contrast to the $HgCdTe$ crystals the $HgMnTe$ crystals keep their surface parameters after mechanical treatment and multiple thermo shock cycles. In order to get the experimental verification of that we have carried out the measurements of surface polariton spectra containing the information about the surface concentration and mobility of the basic charge carriers in the aforementioned crystals before and after mechanochemical and temperature exposures in the wide temperature range.

The temperature dependencies of the surface concentration and mobility of the basic charge carriers were determined from the surface polariton spectra measured by using the well-known attenuated total reflection technique in the millimeter wavelength range (Fig. 9.5, left). The measuring module is shown in Fig. 9.5 (right) along with the different diluted magnetic semiconductors under test.

The results of investigations confirm the legality of the statements expressed above. In particular, it has been determined that in the purest $n-HgMnTe$ ($x = 0.1 \div 0.12$) crystals the surface mobility and concentration of the charge carriers at the temperature $T = 77$ K amount about $\mu \approx 10^5 \text{cm}^2/\text{V} \cdot \text{s}$ and $n \approx 10^{15} \text{cm}^{-3}$ and remain after 300 thermo shock cycles. The typical spectral dependence of the $Al-Hg_{1-x}Mn_xTe$ photodiode is shown in Fig. 9.6.

Schematic view of the photodiode structure profile and a one of the possible topologies of the multi-element structure are shown in Fig. 9.7 (left) and Fig. 9.7 (right), respectively. It is worth noting that along with the two-row multi-element line produced on the $HgMnTe$ crystal and having 64 Schottky photodiodes in each row with the surface active element $50 \times 50 \mu\text{m}^2$ we are able to produce both the single and multi-element photodiodes with the surface active element ranging from $2 \times 2 \text{mm}^2$ to $25 \times 25 \mu\text{m}^2$.

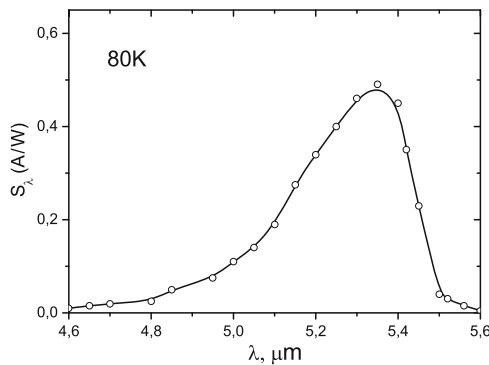


Fig. 9.6 Spectral dependence of photosensitivity of the $Hg_{1-x}Mn_xTe$ ($x \approx 0.12$)-based Schottky photodiode with the Al semitransparent front electrode

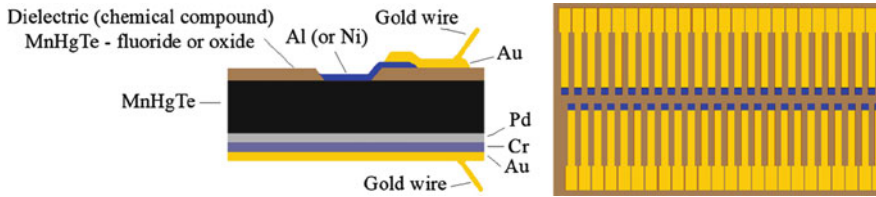


Fig. 9.7 Schottky photodiode structure profile (left) and topology fragment of the multi-element line (right)

9.6 Conclusions

$Hg_{1-x}Mn_xTe$ -based Schottky photodiodes being applicable for $\lambda = 3 \div 5 \mu\text{m}$ and $\lambda = 8 \div 14 \mu\text{m}$ regions have been designed. Our investigation shows that Schottky photodiodes with the $Hg_{1-x}Mn_xTe$ substrate have the technological and circuit advantages in designing the different photodiode matrixes in comparison with the usual $p-n$ junctions in mesas.

Our calculation shows that the peculiarities of the volt-ampere and spectral characteristics of the $Al - Hg_{1-x}Mn_xTe$ Schottky diodes can be explained by the small effective mass of electrons, the narrow-gap band structure and a combination of the tunnel and diffusion currents.

The advantages of the surface parameters of $HgMnTe$ crystals as compared with the $HgCdTe$ ones are proved by the results of the surface polariton spectra processing.

By using the multi-layer structure as the metal-insulator, one can easily design the interelement electric circuits by ensuring the suitable electric switching. Furthermore, such photodiodes keep also their parameters after some hundreds thermo shock cycles due to the enhanced chemical bonds in these crystals.

References

- [1] Tittel, F. K., Curl, R. F., et al.: Recent Advances in Infrared Semiconductor based Chemical Sensing Technologies. In: Proc. of TERA-MIR 2009, p. 1 (2009)
- [2] Vaks, V. L., Illyuk, A. V.: Subterahertz and mid IR spectroscopy of explosive substances. In: Proc. of TERA-MIR 2009, p. 91 (2009)
- [3] Sze, S.: Semiconductor device physics. Mir, Moscow (1984)